Article

Not peer-reviewed version

Artificial Intelligence Algorithm Supporting the Diagnosis of Developmental Dysplasia of the Hip: Automated Ultrasound Image Segmentation

Łukasz Pulik *, Paweł Czech, Jadwiga Kaliszewska, Bartłomiej Mulewicz, Maciej Pykosz, Wiszniewska Joanna, Paweł Łęgosz

Posted Date: 4 August 2025

doi: 10.20944/preprints202508.0091.v1

Keywords: Developmental Dysplasia of the Hip; Graf method; Hip Ultrasound; Artificial Intelligence; Image segmentation; Deep Neural Networks

 doi:10.20944/preprints202508.0091.v1

Article

Artificial Intelligence Algorithm Supporting the Diagnosis of Developmental Dysplasia of the Hip: Automated Ultrasound Image Segmentation

Łukasz Pulik [1,*], Paweł Czech [2], Jadwiga Kaliszewska [3], Bartłomiej Mulewicz [2], Maciej Pykosz [2], Wiszniewska Joanna [2], Paweł Łęgosz [1]

[1] Department of Orthopedics and Traumatology, Medical University of Warsaw, Lindley 4 Str., 02-005 Warsaw, Poland

[2] Pentacomp Systemy Informatyczne S.A., Aleje Jerozolimskie 179 Str., 02-222 Warsaw, 02-222, Poland

[3] Gustav – Children's Clinic, Białej Floty 2 Str., Warsaw, Poland

* Correspondence: lukasz.pulik@wum.edu.pl

Abstract

Background: Developmental dysplasia of the hip (DDH), if not treated, can lead to osteoarthritis and disability. Ultrasound (US) is a primary screening method for the detection of DDH, but its interpretation remains highly operator-dependent. We propose a supervised machine learning (ML) image segmentation model for the automated recognition of anatomical structures in hip US images. **Methods**: A dataset of 10,767 images from 311 patients was annotated for eight key structures according to the Graf method and split into training (75.0%), validation (9.5%), and test (15.5%) sets. Model performance was assessed using the Intersection over Union (IoU) and Dice Similarity Coefficient (DSC). **Results**: The best-performing model was based on the SegNeXt architecture with an MSCAN_L backbone. The model achieved high segmentation accuracy, (IoU; DSC) for chondro-osseous border (0.632; 0.774), femoral head (0.916; 0.956), labrum (0.625; 0.769), cartilaginous (0.672; 0.804) and bony roof (0.725; 0.841). The average Euclidean distance for point-based landmarks (bony rim and lower limb) was 4.8 and 4.5 pixels, respectively, and the baseline deflection angle was 1.7 degrees. **Conclusions**: This ML-based approach demonstrates promising accuracy and may enhance the reliability and accessibility of US-based DDH screening. Future applications could integrate real-time angle measurement and automated classification to support clinical decision-making.

Keywords: developmental dysplasia of the hip; graf method; hip ultrasound; artificial intelligence; image segmentation; deep neural networks

1. Introduction

Developmental dysplasia of the hip (DDH) is the most common musculoskeletal disorder in newborns [1]. It affects approximately 1.4% (95% CI: 0.86 to 2.28) of the world's population, but the incidence of DDH can vary from 0.5% to 30% depending on geographical and ethnic origin [2]. The term DDH reflects a broad spectrum of abnormalities, from mild acetabular deficiency to severe cases with dislocation of the femoral head. In less severe cases, DDH can remain clinically silent in children due to the limited sensitivity and specificity of clinical examination findings, such as hip abduction difference, asymmetric skin creases, or hip instability tests. If not treated, it often leads to the development of hip osteoarthritis (OA) in young adults, which may require total hip arthroplasty (THA) [3]. Up to 40% of patients who undergo THA under 50 years of age have radiological signs of DDH [4]. In severe DDH, symptoms usually appear at birth, including hip instability, shortening of the limb, and limited abduction of the affected hip. In children, we can observe gait problems or a delay in the onset of walking [5]. Conservative treatment (bracing) has the highest success rate if

 doi:10.20944/preprints202508.0091.v1

DDH is diagnosed during the first 6 weeks of life. When the diagnosis is delayed or incorrect, surgery may be necessary [6].

Before the introduction of hip ultrasound (US) by Reinhard Graf (1980s), the diagnosis of DDH was based on clinical examination and radiographic imaging. As mentioned above, clinical examination has only limited efficacy in the detection of DDH, and radiograph-based diagnosis is only possible after 4 to 6 months of age, which is too late for efficient conservative treatment [7]. Today, ultrasound is the gold standard in the diagnosis and monitoring of DDH treatment [8]. Graf's method evaluates acetabulum development by measuring the α angle on standard plane US hip scans. Depending on the α angle hips are classified (I-IV) and the β angle determines the hip subtype. Graf's method is characterized with high sensitivity and specificity in DDH detection, respectively, at 93% (95% CI 0.57-0.99) and 97% (95% CI 0.86-0.99) [9]. However, many errors in the application of the method are reported in the literature, and the use of the Graf method requires experience and strict adherence to the usability checklists [10]. In Europe, many countries have adopted universal ultrasound screening, resulting in a high demand for specialists in the field of DDH diagnosis [8].

The solution for the large volume of US hip scans required could be the recently developed ML-based algorithms. They can improve the reliability of the diagnosis, which is often compromised by the relatively poor quality of the images due to the presence of noise and acquisition errors. They can provide a "second opinion" in diagnosis by standardizing image interpretation and reducing operator-dependent errors [11]. Various diagnostic applications of AI in musculoskeletal ultrasound already include the detection, diagnosis, and prognosis of diseases [12]. The precision of such application of AI in hip US could equal or even outperform that of humans. Some AI-based systems to detect DDH have already been approved by the FDA [13]. However, none of the systems are fully based on the widely accepted Graf rules of image acquisition. In our study, we present a system for automated identification of anatomical structures and landmarks proposed by Graf in two-dimensional (2D) US images. Subsequently, this system could be used in clinical applications to calculate in real time the α and β angles and suggest the possible diagnosis of DDH.

2. Materials and Methods

2.1. Study Materials

The material for image annotation was collected at a private orthopedic clinic during universal screening US scans (4-6 weeks of life) and follow-up visits. All examinations were performed according to the Graf method by six different orthopedic surgeons trained in this method. The data was acquired in the period between January 2022 and December 2023.

The sample material comes from Mindray USG DC-60S, and the settings are individually adjusted by each examiner. Videos (DICOM files) were stored on the PACS server (Mini PACS server HP ProLiant DL20 G10 with processor: E-2224, RAM: 16GB) equipped with Mini mEdivum Electronic Ultrasound Examination Archiving System. All data on DICOM files were anonymized using dedicated automated tool.

The structures were annotated by three independent orthopedic surgeons trained in the Graf method who had participated in a Graf-accredited course. The contours of the anatomical structures in the US images were marked using points along the edges of the target anatomy by dedicated software on selected frames. In the annotation process, a maximum of 25 frames from each video were selected by the reporting physician as the best. Annotating physicians selected structures for marking from a drop-down list among the objects on Checklists I and II according to Prof. Graf, necessary for the assessment of hip joints for DDH (Figure 1). Frames were selected for annotation only when it was possible to mark 5 or more objects. Furthermore, at least one selected frame in each video was classified as diagnostic, according to the Graf methodology (standard plane)[14].

One of the primary ways to reduce the risk of error involved real-time automated feedback. The annotation tool identifies common errors, such as overlap or incorrect region selection in ultrasound images. To reduce subjectivity, each annotated frame was independently reviewed by two physicians

 doi:10.20944/preprints202508.0091.v1

(cross-check). The professionals were trained not only to use the tool, but also to learn from mistakes made in previous batches of annotations. This involved learning from the feedback of independent reviewers and documenting common errors in the form of a shared knowledge base.

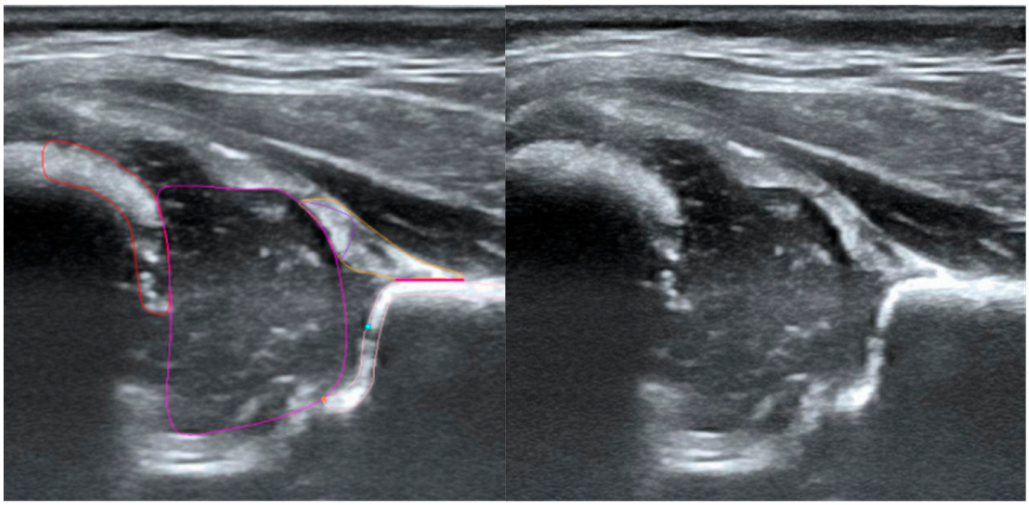

(a) **(b)**

Figure 1. Ultrasound image of the hip in Graf standard plane (a) and labeling of anatomical structures (b). The labeled diagram (b) includes 5 anatomical structures, i.e., chondro-osseous border (red), femoral head (purple), cartilaginous roof (yellow), bony roof (beige), and labrum (light purple). Other landmarks include lower limb (orange), bony rim (light blue), and baseline (pink).

2.2. Artificial Intelligence Model

In our approach, the AI model is trained using supervised learning, which usually allows for the best result, but is very demanding regarding the data gathering and labeling process. The model is presented with a US image from a hip scan and returns a segmentation mask with key anatomical structures that contains five structures and two critical points, marked as squares with a size of 5 pixels and a baseline marked as a segment of 3-pixel thickness. Deep neural networks with gradient descent optimization were used. The specifications of the model architectures are described in a later section.

Two approaches to segmentation were tested. In the first approach (Model-5) data for 5 structures were fed into a segmentation model based on convolutional layers and attention mechanisms. In the second approach (Model-8) the data for five structures were augmented with two points (lower limb and bony rim) and the baseline. In both models, five different architectures were tested, and the best one was selected. We tested the following: SegFormer [15], OCRNet [2], U-Net [16], U-HRNet [17] and SegNeXt [18] (Supplementary Table 1). For each architecture, there were many training settings (described in the results section). Among the many architectures and settings, the one with the best Intersection over Union (IoU) was used.

Additionally, during the model training process, the PaddleSeg library uses various pre-processing techniques (e.g. Resize, Normalize) and augmentation techniques (e.g. RandomHorizontalFlip, RandomDistort), which were also used in our training. The first step of pre-processing involved cropping the images to the ultrasound area to eliminate regions that do not pertain directly to the ultrasound scan. The second step involved the preparation of masks containing only 5 classes (chondro-osseous border, femoral head, labrum, cartilaginous roof and bony roof). This step was performed to create the input for Model-5 (Figure 2).

 doi:10.20944/preprints202508.0091.v1

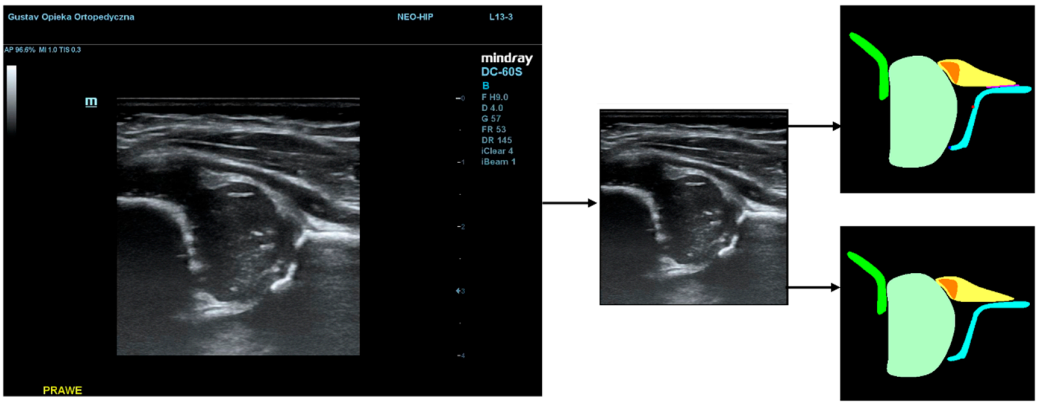

Figure 2. Result of pre-processing: extracting the USG area from the image and preparing masks for Model-5 (lower picture) and Model-8 (upper picture).

For segmentation labels from models, post-processing was used, which removed artifacts related to multiple instances of a single class caused by either small regions that needed to be cleaned or divided areas that should be connected. Moreover, mistakes for regions that were not properly marked by the model were also corrected. The best image had to be selected for post-processing. Selection was made based on a scoring algorithm which evaluated the quality of the segmentation mask and the correctness of the US image itself, whether it had all the necessary classes visible and whether it presented a Graf standard plane.

The evaluation of models is crucial for understanding their effectiveness. In the field of image segmentation, one of the most widely adopted metrics is Intersection over Union (IoU). It quantifies the overlap between the predicted segmentation mask and the ground truth mask for a specific object class. Mathematically, IoU is defined as the ratio of the area of intersection between the predicted and ground truth regions to the area of their union. Formally, for a given class C, the IoU can be expressed as:

$$IoU(C) = \frac{|\mathrm{A} \cap \mathrm{B}|}{|\mathrm{A} \cup \mathrm{B}|}$$

where A represents the area of the predicted segmentation mask and B denotes the area of the ground truth mask. The intersection |A∩B| represents the area where both masks overlap, while the union |A∪B| represents the total area covered by at least one of the masks. A higher IoU value indicates better model performance. To evaluate the models the mean Intersection over Union for a specific class across an entire dataset was computed. Another metric we used is the dice similarity coefficient (DSC) that ranges from 0 to 1. Here, A represents the predicted point set and B the labeled point set.

$$\mathrm{DSC}\ (\mathrm{SA}, \mathrm{SP}) = \frac{2 \cdot |A\ B|}{|A|\ +\ |B|}$$

All images were split into three sets: training set (for model learning), validation set (to select the best training iteration), and test set (to choose the best model among tested architectures and for final model evaluation). Images related to the same patient had to appear in only one of the sets. The split was performed in such a way that the test and validation set each contained approximately 10% of the videos (Table 1).

Given the dependency between paired observations and non-normal distribution, the Wilcoxon signed-rank test, a non-parametric alternative to the paired t-test, was employed. To control for the family-wise error rate resulting from multiple comparisons, the Bonferroni correction was applied, with the significance threshold set at α = 0.01. All statistical analyses were performed using Python version 3.9.13 with the SciPy library (version 1.7.3).

 doi:10.20944/preprints202508.0091.v1

Table 1. Numerical and percentage share of data sets (with column percentages).

	Videos n (%)	Images n (%)
Test set	93 (13.6%)	1671 (15.5%)
Validation set	72 (10.5%)	1022 (9.5%)
Training set	520 (75.9%)	8074 (75.0%)

4. Results

The dataset consisted of 375 female and 310 male US hip scans. Dysplastic hips (DDH) or physiologically immature hips (type IIa+) were diagnosed with 106 (15.47%) of all 685 DICOM files. The descriptive statistics for dataset are presented in Table 2.

Table 2. Descriptive statistics of study population (with row percentages).

	Age, days*	Female (%)
Test set	49 (40-75)	70 (75.3%)
Validation set	58 (40-79)	40 (55.6%)
Training set	47 (40-70)	265 (51.0%)

** Median (IQ range).*

The accuracy of the model was evaluated using the IoU metric. The average value of this metric was calculated based on the test dataset for 5 classes (chondro-osseous border, femoral head, labrum, cartilaginous roof, and bony roof). For classes representing points (bony rim and lower limb), the Euclidean distance from the centroid of the model's segment to the centroid of the doctor's segment was calculated. For the baseline class, the angle of deviation between the doctor's baseline and the model's baseline was computed. Two models were analyzed: Model-8 (generating segments for 8 classes) and Model-5 (generating segments for 5 classes). The analysis revealed statistically significant differences between the models in classes 1, 3, and 4. In class 1, the 8-class model demonstrated superior performance, whereas in classes 3 and 4, the 5-class model achieved higher IoU scores compared to the 8-class model. Despite reaching statistical significance, the observed effect sizes ranged from small to moderate, indicating only moderate practical relevance of these differences. The average values of the metrics calculated for the test dataset for each class are presented in Table 3.

Table 3. Average metric values for each class for both models.

	Model-8	Model-5	P-value
1. Chondro-osseous border (IoU)	0.632	0.624	<0.001
2. Femoral head (IoU)	0.916	0.915	0.26
3. Labrum (IoU)	0.621	0.625	<0.01
4. Cartilaginous roof (IoU)	0.666	0.672	<0.001
5. Bony roof (IoU)	0.716	0.725	0.89
6. Bony rim (Euclidean distance) [pixels]	4.8	-	
7. Lower limb (Euclidean distance) [pixels]	4.5	-	
8. Baseline (deflection angle) [degrees]	1.7	-	

To evaluate the effectiveness of the segmentation model, the success rate was calculated, defined as the percentage of frames in which the doctor annotated a given class and for which the Intersection over Union (IoU) between the doctor's annotation and the model prediction reaches a value of at least 0.5 (true positives). The results are presented in Table 4.

 doi:10.20944/preprints202508.0091.v1

Table 4. Success rate for each class for both models.

	Model-8	Model-5
Chondro-osseous border	85.88%	84.56%
Femoral head	100.00%	100.00%
Labrum	82.41%	85.76%
Cartilaginous roof	97.79%	98.50%
Bony roof	97.85%	98.03%

** Median (IQ range).*

Furthermore, for 5 classes (chondro-osseous border, femoral head, labrum, cartilaginous roof, and bony roof), the dice similarity coefficient on the test dataset was calculated. The average values of the metrics for each class are presented in Table 5.

Table 5. Dice similarity coefficient for each class for both models.

	Model-8	Model-5
chondro-osseous border	0.774	0.769
femoral head	0.956	0.956
labrum	0.767	0.769
cartilaginous roof	0.799	0.804
bony roof	0.834	0.841

** Median (IQ range).*

The model that achieved the highest segmentation accuracy was based on the SegNeXt architecture with the MSCAN_L backbone. SegNeXt is a convolutional network that features hierarchical attention mechanisms (HAM), which contribute to its high segmentation accuracy [18]. The training parameters of our best model are detailed in Supplementary Table S2.

To illustrate the performance of the segmentation model, a comparison is presented between the labels obtained by the segmentation model and the ground truth labels. Two models were analyzed: Model-8 (generating segments for 8 classes) and Model-5 (generating segments for 5 classes). Both the cases with the highest quality model labels and the cases where the model labels were less accurate are presented. Figure 3 shows one of the best cases, in which Model-5 and Model-8 accurately labeled the classes relative to the doctor's labels. The worst-case scenario was also analyzed, in which the prediction results differ significantly from the ground truth labels (Figure 4).

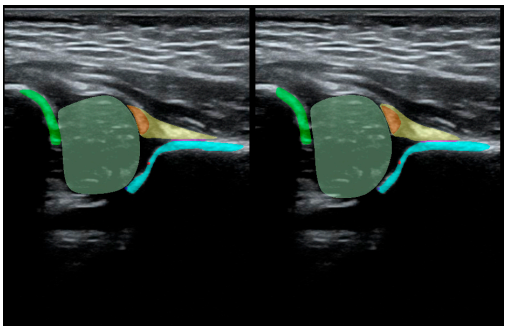

 doi:10.20944/preprints202508.0091.v1

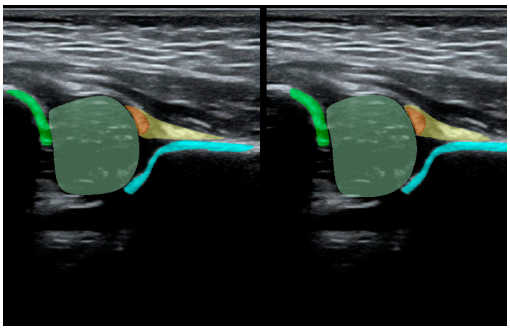

Figure 3. High quality model labels (upper - Model-8) and (lower - Model-5). Annotated mask on the left, model mask on the right.

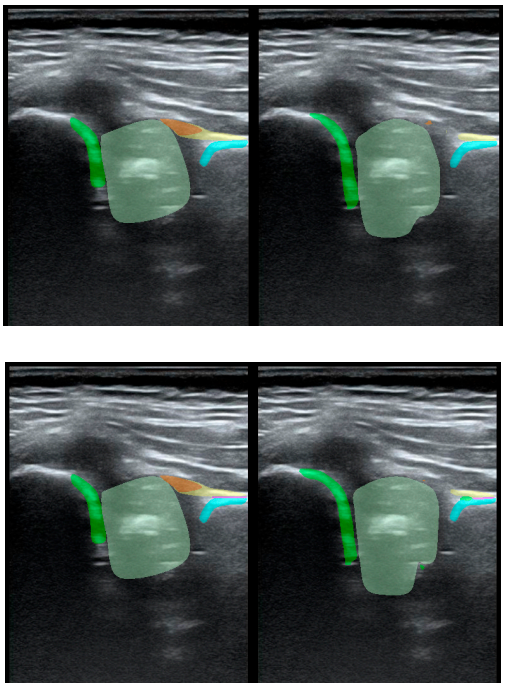

Figure 4. Low-quality model labels (upper - Model-8) and (lower - Model-5). Annotated mask on the left, model mask on the right.

5. Discussion

In our work, orthopedic surgeons annotated all the structures recommended by Graf to obtain reproducible results. We expect that the structures obtained in this way can be used to make a reliable clinical diagnosis regarding the type of hip joint in the future. Some studies such as Quander et al. and Hareendranathan et al. use a different approach and analyze the geometry of structures instead of supervised learning methods [19] . Multiple authors analyze 3D US scans, but the methodology proposed by Graf is based on 2D US [20,21]. According to the literature, the sensitivity [95%CI] of such AI US-based systems can be as high as 0.98 [0.91-1.00]. Their specificity [95%CI] is also reported to be high - 0.95 [0.81-0.99] [22].

Sezer et al. used 675 annotated US frames with 'iliac wing', 'labrum', and acetabulum. The R-CNN (Mask Region-Based Convolutional Neural Network) method was used. The authors do not report the results as an IoU metric. Instead, they report a success rate that is IoU of ≥0.5 (true positive). The average success rate was 98.25% for the iliac wing, 94.91% for the acetabulum and 97.72% for the labrum [23]. Our success rate for the bony roof, which represents acetabulum and iliac wing, ranged

 doi:10.20944/preprints202508.0091.v1

from 97.85% (Model-8) to 98.03% (Model-5). For the labrum, our model had a success rate ranging from 82.41% (Model-8) to 85.76% (Model-5).

Chen et al. described the use of an improved fully convolutional neural network to identify the femoral head on US images. The raw dataset consisted of 55 labeled US images of hip joints. The authors used the Cascaded FNet method and extracted region of interest (ROI). The model achieved an IoU of 0.897 [24]. Our models achieved IoU for the femoral head ranging from 0.915 (Model-5) to 0.916 (Model-8).

Li et al. used 400 US Graf standard plane images for a semi-supervised deep learning method based on a feature pyramid network (FPN) and a contrastive learning scheme based on a Siamese architecture. The annotations included the junction of cartilage and bone (chondro-osseous border), hyaline cartilage (cartilaginous roof), acetabular roof (bony roof), femoral head, joint capsule, labrum, ilium, bony part of the acetabular roof, synovial fold. However, the authors did not include the lower limb and bony rim which are necessary for US scan assessment according to Graf [25]. For the chondro-osseous border, the authors achieved DSC ranging from 0.685 to 0.864. Our model DSC ranged from 0.769 (Model-5) to 0.774 (Model-8). For the femoral head, the authors achieved a DSC of 0.860 - 0.899 and our result was 0.956 (both Model-5 and Model-8). For the labrum, the DSC in Li et al. was 0.570 - 0.814 and our result was 0.767 (Model-8) - 0.769 (Model-5). For the cartilaginous roof the DSC in Li et al. was 0.000 - 0.565 while our results were 0.799 (Model-8) - 0.804 (Model-5). For the ilium and lower ilium, the authors' results were 0.6802 - 0.854 and 0.379 - 0.819 respectively, and our result for the bony roof that combines both structures was 0.834 (Model-8) - 0.841 (Model-5).

Stamper et al. was based on 190 US hip scans. The annotations included the femoral head, ilium, and labrum. U-Net was used to segment key anatomical structures. However, this study was aimed at automating femoral head coverage (FHC) calculation for DDH screening and ours was focused on the Graf method [26]. The authors reported DSC for the femoral head of 0.924 and our result was 0.956 (both Model-8 and Model-5). The result for the ilium was 0.857 and ours for the bony roof was 0.834 (Model-8) - 0.841 (Model-5). For the labrum Stamper et al. achieved a DSC of 0.710 our result was 0.767 (Model-8) and 0.769 (Model-5).

Hu et al. used Mask R-CNN on 1,231 US images of the infant hip from 632 patients and annotated the flat Ilium, lower limb, labrum, CO junction (chondro-osseous border), bony rim, lower limb point, and midpoint of labrum. For the chondro-osseous border the authors achieved a DSC ranging from 0.829 to 0.873 [27]. Our model DSC ranged from 0.769 (Model-5) to 0.774 (Model-8). For the labrum, the DSC of Hu et al. was 0.791 - 0.841 and our result was 0.767 (Model-8) - 0.769 (Model-5). For the ilium and lower limb (marked as an area and part of the bony roof) the results were 0.869 - 0.869 and 0.809 - 0.838 - respectively and our result for the bony roof that combines both structures was 0.834 (Model-8) - 0.841 (Model-5).

Golan et al. used the DCNN network and GAN. The authors chose a unique approach in which 1,056 US scans of infant hips were annotated by crowdsourcing to crowdFlower platform users. The annotated structures were the ilium and acetabular roof, but the authors do not report DSC or the IoU metric [28].

Lee et al. analyzed 1,243 hip US images from 168 infants. Mask annotations were made using the Computer Vision Annotation Tool (CVAT). The annotated structure was a combined area of bony roof and cartilaginous roof marked on a Graf standard plane. The Authors do not report the DSC or IoU [29].

Our study is the only one that implements the identification of all anatomical structures required by the Graf method to assess a 2D US. We achieved similar or better IoU, DSC, and success rate compared to other identified studies.

In future studies, we plan to design a complete CDSS class system (Clinical Decision Support System) to support doctors in their complex decision-making processes regarding DDH diagnosis and management. Recently CDSS have seen a rapid evolution and they are now commonly administered through computerized clinical workflows and medical records [30]. The system will be based on a machine learning (ML) algorithm that measures the α and β angles in strict accordance

 doi:10.20944/preprints202508.0091.v1

with the Graf method. Other data such as patient demographics, potential risk factors for DDH, and clinical examination results will also be collected and analyzed. Further benefits of artificial intelligence (AI) in ultrasound imaging may include improved diagnostic accuracy leading to better patient outcomes.

Supplementary Materials: The following supporting information can be downloaded at the website of this paper posted on Preprints.org

Author Contributions: Conceptualization: Ł.P. and J.K.; Methodology: P.C., B.M., M.P. and W.J; Software: P.C., B.M., M.P. and W.J.; Resources: Ł.P, P.Ł., J.K.; Writing - original draft preparation: Ł.P., P.C., J.K., B.M., M.P. and W.J; Writing - review and editing: Ł.P., P.C., J.K., B.M., M.P., P.Ł. and W.J; Visualization: B.M., M.P. and Ł.P.; Supervision: P.C. and Ł.P.; Project administration: J.K, P.C.; Funding acquisition: J.K. All authors have read and agreed to the published version of the manuscript.

Funding: This research was funded by the Polish Medical Research Agency (ABM), grant number 2022/ABM/02/00004. The Article Publication Charges were funded by Medical University of Warsaw.

Data Availability Statement: The data that support the findings of this study are available from Pentacomp Systemy Informatyczne S.A but restrictions apply to the availability of these data, which were used under license for the current study, and so are not publicly available. Data are however available from the authors upon reasonable request and with permission of Pentacomp Systemy Informatyczne S.A.

Conflicts of Interest: The co-authors are employees (Paweł Czech, Jadwiga Kaliszewska, Bartłomiej Mulewicz, Maciej Pykosz, Wiszniewska Joanna) or cooperate (Łukasz Pulik, Jadwiga Kaliszewska), with of Pentacomp Systemy Informatyczne S.A. that may benefit from the development of products as an outcome of the work. The authors state no other conflicts of interest.

Institutional Review Board Statement: This study was conducted in accordance with the Declaration of Helsinki. The Ethics Committee of the Medical University of Warsaw (AKBE/07/2022) approved the study protocol and waived the requirement for informed consent due to its retrospective design.

Informed Consent Statement: Not applicable, retrospective observational study.

References

1. Pulik Ł, Płoszka K, Romaniuk K, Sibilska A, Jedynak A, Tołwiński I, et al. Impact of Multiple Factors on the Incidence of Developmental Dysplasia of the Hip: Risk Assessment Tool. Medicina. 2022;58(9):1158.
2. Tao A, Sapra K, Catanzaro B. Hierarchical multi-scale attention for semantic segmentation. arXiv preprint arXiv:200510821. 2020.
3. Subaşı İÖ, Veizi E, Çepni Ş, Alkan H, Oğuz T, Fırat A. Clinical Examination Findings Can Accurately Diagnose Developmental Dysplasia of The Hip—A Large, Single-Center Cohort. Children [Internet]. 2023; 10(2).
4. Muddaluru V, Boughton O, Donnelly T, O'Byrne J, Cashman J, Green C. Developmental dysplasia of the hip is common in patients undergoing total hip arthroplasty under 50 years of age. SICOT-J. 2023;9:25.
5. Anable NR, Luginsland LA, Carlos C, Stevens Jr WR, Loewen AM, Jeans KA, et al. Investigating pelvic drop gait abnormality in adolescent hip pathology patients. Gait & Posture. 2024;110:65-70.
6. He J, Chen T, Lyu X. Analysis of the results of hip ultrasonography in 48 666 infants and efficacy studies of conservative treatment. Journal of Clinical Ultrasound. 2023;51(4):656-62.
7. Kitay A, Widmann RF, Doyle SM, Do HT, Green DW. Ultrasound is an Alternative to X-ray for Diagnosing Developmental Dysplasia of the Hips in 6-Month-Old Children. HSS Journal®. 2019;15(2):153-8.
8. Krysta W, Dudek P, Pulik Ł, Łęgosz P. Screening of Developmental Dysplasia of the Hip in Europe: A Systematic Review. Children (Basel). 2024;11(1).

 doi:10.20944/preprints202508.0091.v1

9. Chavoshi M, Mirshahvalad SA, Mahdizadeh M, Zamani F. Diagnostic Accuracy of Ultrasonography Method of Graf in the detection of Developmental Dysplasia of the Hip: A Meta-Analysis and Systematic Review. Arch Bone Jt Surg. 2021;9(3):297-305.
10. Ossendorff R, Placzek S, Bornemann R, Walter SG. Four decades of the Graf method in screening for developmental dysplasia of the hip (part I): Rightly the gold standard or of dubious benefit? Frontiers in Pediatrics. 2022;10.
11. Micucci M, Iula A. Recent Advances in Machine Learning Applied to Ultrasound Imaging. Electronics. 2022;11(11):1800.
12. Hattori S, Saggar R, Heidinger E, Qi A, Mullen J, Fee B, et al. Advances in Ultrasound-Guided Surgery and Artificial Intelligence Applications in Musculoskeletal Diseases. Diagnostics. 2024;14(18):2008.
13. Jaremko JL, Hareendranathan A, Bolouri SES, Frey RF, Dulai S, Bailey AL. AI aided workflow for hip dysplasia screening using ultrasound in primary care clinics. Scientific Reports. 2023;13(1):9224.
14. Graf R, Mohajer M, Plattner F. Hip sonography update. Quality-management, catastrophes â€“tips and tricks. Medical ultrasonography. 2013;15(4):299-303.
15. Xie E, Wang W, Yu Z, Anandkumar A, Alvarez JM, Luo P. SegFormer: simple and efficient design for semantic segmentation with transformers. Proceedings of the 35th International Conference on Neural Information Processing Systems: Curran Associates Inc.; 2024. p. Article 924.
16. Huang H, Lin L, Tong R, Hu H, Zhang Q, Iwamoto Y, et al., editors. Unet 3+: A full-scale connected unet for medical image segmentation. ICASSP 2020-2020 IEEE international conference on acoustics, speech and signal processing (ICASSP); 2020: IEEE.
17. Wang J, Long X, Chen G, Wu Z, Chen Z, Ding E. U-hrnet: delving into improving semantic representation of high resolution network for dense prediction. arXiv preprint arXiv:221007140. 2022.
18. Zhang Y, Yao T, Qiu Z, Mei T. Lightweight and progressively-scalable networks for semantic segmentation. International Journal of Computer Vision. 2023;131(8):2153-71.
19. Quader N, Hodgson AJ, Mulpuri K, Schaeffer E, Abugharbieh R. Automatic Evaluation of Scan Adequacy and Dysplasia Metrics in 2-D Ultrasound Images of the Neonatal Hip. Ultrasound Med Biol. 2017;43(6):1252-62.
20. Quader N, Hodgson A, Mulpuri K, Cooper A, Abugharbieh R. Towards reliable automatic characterization of neonatal hip dysplasia from 3D ultrasound images. International Conference on Medical Image Computing and Computer-Assisted Intervention; 2016: Springer.
21. Paserin O, Mulpuri K, Cooper A, Hodgson AJ, Garbi R, editors. Real time RNN based 3D ultrasound scan adequacy for developmental dysplasia of the hip. Medical Image Computing and Computer Assisted Intervention–MICCAI 2018: 21st International Conference, Granada, Spain, September 16-20, 2018, Proceedings, Part I; 2018: Springer.
22. Chen M, Cai R, Zhang A, Chi X, Qian J. The diagnostic value of artificial intelligence-assisted imaging for developmental dysplasia of the hip: a systematic review and meta-analysis. Journal of Orthopaedic Surgery and Research. 2024;19(1):522.
23. Sezer A, Sezer HB. Segmentation of measurable images from standard plane of Graf hip ultrasonograms based on Mask Region-Based Convolutional Neural Network. Joint Diseases and Related Surgery. 2023;34(3):590.
24. Chen L, Cui Y, Song H, Huang B, Yang J, Zhao D, et al. Femoral head segmentation based on improved fully convolutional neural network for ultrasound images. Signal, Image and Video Processing. 2020;14:1043-51.

 doi:10.20944/preprints202508.0091.v1

25. Li X, Zhang R, Wang Z, Wang J. Semi-supervised learning in diagnosis of infant hip dysplasia towards multisource ultrasound images. Quantitative Imaging in Medicine and Surgery. 2024;14(5):3707.
26. Stamper A, Singh A, McCouat J, Voiculescu I, editors. Infant hip screening using multi-class ultrasound scan segmentation. 2023 IEEE 20th International Symposium on Biomedical Imaging (ISBI); 2023: IEEE.
27. Hu X, Wang L, Yang X, Zhou X, Xue W, Cao Y, et al. Joint landmark and structure learning for automatic evaluation of developmental dysplasia of the hip. IEEE Journal of Biomedical and Health Informatics. 2021;26(1):345-58.
28. Golan D, Donner Y, Mansi C, Jaremko J, Ramachandran M, CUDL, editors. Fully automating Graf's method for DDH diagnosis using deep convolutional neural networks. Deep Learning and Data Labeling for Medical Applications: First International Workshop, LABELS 2016, and Second International Workshop, DLMIA 2016, Held in Conjunction with MICCAI 2016, Athens, Greece, October 21, 2016, Proceedings 1; 2016: Springer.
29. Lee S-W, Ye H-U, Lee K-J, Jang W-Y, Lee J-H, Hwang S-M, et al. Accuracy of new deep learning model-based segmentation and key-point multi-detection method for ultrasonographic developmental dysplasia of the hip (DDH) screening. Diagnostics. 2021;11(7):1174.
30. Sutton RT, Pincock D, Baumgart DC, Sadowski DC, Fedorak RN, Kroeker KI. An overview of clinical decision support systems: benefits, risks, and strategies for success. NPJ digital medicine. 2020;3(1):17.